New Approach for Ultrasound-Guided Regional Analgesia of Brachial Plexus in Egyptian Donkeys

Adel Sobhy[1], Ahmed El-khamary[1], Ahmed M. Rashwan[2,3] Ashraf Shamaa[4], Mostafa Kassem[5], Mohamed M. A. Abumandour[6]*, Ahmed El-Mansi[7, 8] and Ahmed G. Nomir[2]

[1]Department of Surgery, Faculty of Veterinary Medicine, Damanhour University, Damanhour 22511, Egypt.
[2]Department of Anatomy and Embryology, Faculty of Veterinary Medicine, Damanhour University 2511, Egypt.
[3]Department of Life Science Frontiers, Center for iPS Cell Research and Application, Kyoto University, Kyoto, Japan.
[4]Department of Surgery, Faculty of Veterinary Medicine, Cairo University, P.O. Box 12613, Giza, Egypt.
[5]Department of Surgery, Faculty of Veterinary Medicine, Alexandria University, Alexandria, Egypt.
[6]Department of Anatomy and Embryology, Faculty of Veterinary Medicine, Alexandria University, Alexandria, Egypt.
[7]Biology Department, College of Science, King Khalid University, Abha, Saudi Arabia
[8]Zoology Department, Faculty of Science, Mansoura University, Mansoura, Egypt

ABSTRACT

It's important to have a novel ultrasound (US)-guided approach to brachial plexus block since it allows for a better understanding of the surface anatomy and relationships, as well as injury and consequences. This study used three methodologies of approach (anatomical, cadaveric, and live experimental tests) to describe the brachial plexus topography in the donkey, evaluate the US color doppler brachial plexus blockage, and test the analgesic efficacy. We topographically anatomized the brachial plexus in three cadavers. Color Doppler US-guided methylene blue dye was injected into both sides of the brachial plexus: p1 (plexus root 4±0.5 cm above the greater tuberosity) and p2 (division site of all plexus nerves) of six cadavers. Finally, the live experimental study involved brachial plexus injections at both sides of p1 and p2 (standing position). Our results from the cadaveric US showed that the brachial plexus root was sufficiently stained at site p1 as opposed to site p2. In the live experimental study, the brachial plexus appeared as a hyperechoic cluster at the p1 site, while the large and small rounded regions at the p2 site were hypoechoic. The distance at site P1 was 4.8±0.2 cm using 15 ml of Lidocaine local anesthetic solution for blockage. However, the distance at site p2 was 6.8±0.2 cm, and 25 ml of local anesthetic was sufficient for complete nerve blockage. We concluded that by using the color-doppler US-guided for the brachial plexus injection, site p1 was more efficient and avoided vascular penetration than site p2.

* Corresponding author: m.abumandour@yahoo.com, M.abumandour@alexu.edu.eg
0030-9923/2023/0001-0001 $ 9.00/0

INTRODUCTION

The donkey (*Equus asinus*), is an essential part of farming and agriculture, especially in poor nations where it is one of the most affordable modes of transportation for farmers (Food and Agriculture Organization of the United Nations, 2021), with the largest increase in donkey population noted in the sub-Saharan African region (Norris *et al*., 2021). Nevertheless, the scientific information available for this species remains limited.

The brachial plexus consists of the ventral branches

of the C5-T2 spinal nerves (Campoy *et al*., 2010; Dyce *et al*., 2010; Lemke and Creighton, 2008). It extends as a large band of nervous tissue, having its caudal boundary in contact with the superior surface of the first rib, then the plexus crosses between the two segments of the scalenus muscle (Atiba *et al*., 2019). The plexus sweeps through the axilla and splits into the following branches: suprascapular, sub-scapular, musculocutaneous, radial, median, ulnar axillary, thoracodorsal, thoracic lateral, pectoral, and long thoracic nerves (Dyce *et al*., 2010; Mahler and Adogwa, 2008). The radial, median, ulnar, and musculocutaneous nerves are the main nerves supplying the forelimb (Dyce *et al*., 2010; Souto *et al*., 2020).

A well-validated technique that is used for forelimb sensory and motor blockade is the brachial plexus block (Monticelli *et al*., 2018; Raw *et al*., 2013). In most cases, the procedure is effective when using surgical analgesia in treating the front limb distal to the shoulder. It is clinically relevant because it reduces the risks of using general anesthesia (Mirza and Brown, 2011). The traditional axillary approach to brachial plexus block is carried out using a needle positioning guide with anatomical landmarks (conventional blind techniques) (Mahler and Adogwa, 2008; Monticelli *et al*., 2018; Raw *et al*., 2013). Complications associated with blind brachial plexus blockade include unilateral blockade of the phrenic nerve, intravascular injection (Bennett *et al*., 2020), pneumothorax (Bhalla and Leece, 2015), Horner syndrome (Bennett *et al*., 2020; Holzman, 2002), and ventricular arrhythmias (Adami and Studer, 2015).

However, the ultrasound (US) imaging techniques allow precise needle location and real-time monitoring of the delivery of the local anesthetic solution (Bennett *et al*., 2020; Campoy *et al*., 2010; Marhofer *et al*., 1997). The benefits of this are improved efficacy of the nerve block, faster onset times, and smaller amounts of local anesthetic solution required to produce an effective block (Brull *et al*., 2007; Marhofer *et al*., 1997, 2005). Confirming the local anesthetic distribution around the target nerve is the most significant advantage of US for a peripheral nerve block (Marhofer *et al*., 2005). This significantly differentiates it from the conventional blind techniques, which can fail because the local anesthesia was not uniformly distributed to the target nerve (Brull *et al*., 2007; Tsui *et al*., 2009). The use of the US-guided brachial plexus nerve block technique in donkeys using a volume of 25mL of lidocaine per injection site (Atiba *et al*., 2019) was one of the available cited researches. Therefore, our work was designed to illustrate and evaluate a new ultrasound-guided approach that precisely locates the plexus and avoids the dire consequences of damage to the nerves and surrounding structures.

MATERIALS AND METHODS

Animals

Our experimental study was done on nine donkey cadavers (3 for topographical anatomical study and 6 for ultrasound-guided cadaver study), six healthy male and female donkeys having a bodyweight of 170±10 kg and ages ranging between 4-6 years. All procedures were carried out at the Damanhour University Department of Surgery in the Faculty of Veterinary Medicine.

Animal welfare/ethical statement

The Animal Care and Use Ethical Committee of the Faculty of Veterinary Medicine, Damanhour University, accepted the experimental protocol.

Topographical anatomical study

To determine the anatomical landmarks, their related structures, and the appropriate approach to the brachial plexus, the cadaver was placed in the lateral recumbency position. The humerus, shoulder joint and jugular vein were identified, and we made a longitudinal incision of the skin parallel to the first rib, the shoulder joint, and the scapula-dorsal part. The skin was separated and reflected dorsally and ventrally to expose the subcutaneous fascia from the underlining fascia. Superficial and deep pectoral muscles originating in the sternum, brachiocephalic muscle cranially, trapezius-rhomboids dorsally, and serratus anterior were carefully dissected from their scapular attachment. The nerve and blood vessels were exposed after the removal of all fatty layers and connective tissues in the axillary space. The brachial plexus was recognized, and the eleven nerves were identified at the axilla ventral border. The Vernier caliper (0-150mm) was used to measure the distance from the skin to the probe position site.

US-guided technique (cadaveric study)

In the lateral recumbent position of the cadaver, the cranial border and the ventral part of the scapular were clipped. The US gel was applied and the transducer at 7.5-12 MHz was used linearly, placing it directly above the subcutaneous fascia, brachiocephalic, and sternocephalic muscles, which appeared to be the hypoechoic and non-echoic areas of the axillary and venous arteries. The transducer moved 2-3cm dorsally until the concave surface ridge appeared in the region. The area was scanned for the appearance of hyperechogenic threads. Site p1 was 2cm above the greater tuberosity of the humerus representing the caudal aspect of the brachial plexus while site p2 was 5cm above the greater tuberosity of the humerus, representing the cranial aspect, of the brachial plexus and

indicating the bifurcation of the plexus to different nerves. This area was scanned over the greater tuberosity of the humerus and divided into two parts, site p1 and site p2. A spinal needle with a 90mm (22-gauge) stylet was inserted deeply close to the US transducer in the longitudinal axis of the US beam above the greater tubercle, in both sites. The ventromedial direction of the needle was used. 1ml of methylene blue was injected at both sites. We scored each injection for the 12 attempts as follows: 0 = non-stained nerve (miss = 0%), 1 = partial stained nerve (30-40%), 2 = completely stained nerve (50-100%) and record of penetration at the surrounding structure. The stained segment of the nerve was recorded.

US-guided approach (live experimental study)

The animals were sedated using xylazine HCl 2% (Xyla-Ject, ADWIA Pharmaceuticals Co. Cairo, Egypt) at 1.1 mg/kg intravenously. The examined area of the scapula's cranial border was clipped, shaved, and disinfected with alcohol. 4ml of lidocaine was subcutaneously injected at the target site, and the sensation in the forelimb was verified laterally, caudally, and medially using a 22-gauge 5 mm needle via a pinprick test. To identify the pain response, the study observed the actions associated with limb lifting, whining, and attempting to bite or move another part of the body. The US gel and transducer were placed in the area above the greater tuberosity of the humerus at the cranial border of the scapula and moved until the brachial plexus was identified at two sites: P1 and P2. Scanning continued until hyper-echogenic threads and blood vessels were identified. Under the guidance of Doppler US, the needle was inserted ventro-medially, then syringe aspiration was performed for confirmation that the needle was not inserted in any surrounding artery or vein. 10ml of Lidocaine (Debocaine 2% Al-Debeiky Pharmaceutical Industries Co., Egypt) was injected under the guidance of the Doppler US at site P1 and 20ml of lidocaine was injected at site P2. For the achievement of pain stimulus to the needle and loss of sensation, the pinprick test was applied to the lateral aspect of the shoulder region to test the effect of anesthesia.

RESULTS

Anatomy of brachial plexus

The brachial plexus is observed anatomically parallel to the first rib, just above the greater tuberosity of the humerus. The root of the plexus was located at about 2±0.5 cm above the tuberosity (recorded as site P1) and the division of all the plexus nerves was identified at about 4±0.5 cm above the tuberosity, representing site P2 (Figs. 1, 2). The axillary vessels and all nerves linked to the

brachial plexus were clearly identified from the overlying connective tissue (CT) and fat. The identified eleven (11) nerves included pectoral nerves (cranial and caudal parts), suprascapular, subscapular, musculocutaneous, axillary, thoracodorsal, long thoracic, median, ulnar, and radial nerves. The distance from the skin to the target plexus that all nerves were clearly identified from their origin to the divisions was 5±0.5 cm at site P1 and 7±1.0 cm at site P2 (Fig. 3).
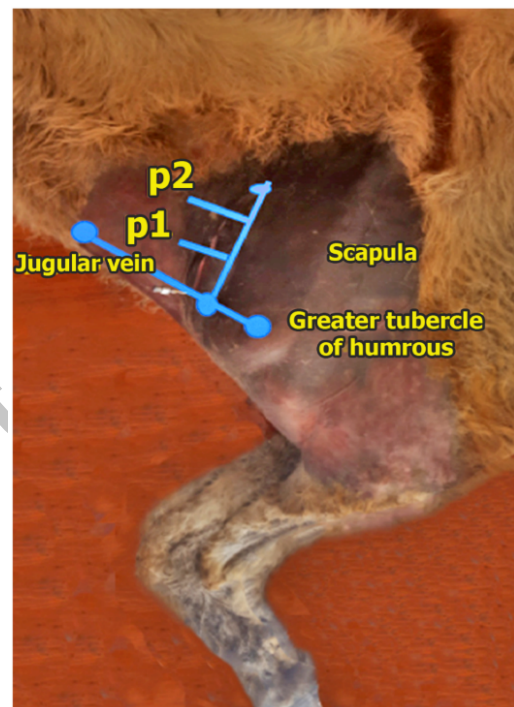

Fig. 1. Gross anatomical image to determine the site of brachial plexus and anatomical landmarks. First-line from the greater tuberosity of the humerus to the jugular vein, the second line is perpendicular to the first line parallel to the first rib and scapula which determines two sites P1 and P2.

Fig. 2. Gross anatomical image in which the A determines the position of probe at p1 of brachial plexus while the B determines the position of probe at p2 of brachial plexus.
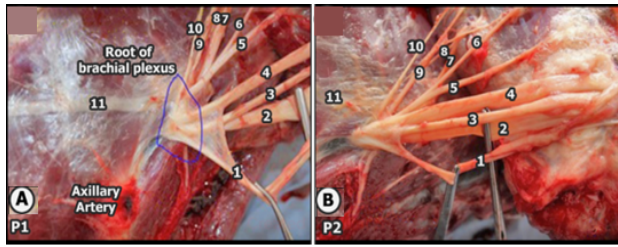
Fig. 3. Gross Anatomical image of the brachial plexus and its branches. A shows determines the anatomical dissection of the root of the brachial plexus at site P1 with the appearance of an axillary artery, while B shows determines the anatomical dissection of the brachial plexus after bifurcation from the origin at site P2.

Abbreviations: 1, musculocutaneous nerve; 2, median nerve; 3, the ulnar nerve; 4, radial nerve; 5, axillary nerve; 6, lateral thoracic nerve; 7, suprascapular nerve; 8, subscapular nerve; 9, caudal pectoral nerve; 10, dorsal thoracic nerve; and long 11, thoracic nerve.

US-guided cadaver study of brachial plexus

The greater tuberosity of the humerus was used as an anatomical landmark. The area above greater tuberosity was scanned with the transducer, and the skin and superficial pectoral region at site P1 appeared to be hypoechoic. A non-echoic center identified with a hyperechoic rim indicated the axillary vessels. The identified hyperechoic clustering structure was the brachial plexus, which was located 4.8±0.4 cm from the skin. Four large rounded hyperechoic structures measuring about 6.8±0.2 cm at site P2 were identified as the median nerve, radial nerve, ulnar nerve, and musculocutaneous nerve (Fig. 4). The puncture site was identified through the brachiocephalic and sternocephalic muscles until it reached the area of the brachial plexus, which was stained with methylene blue. The stain was distributed in the cranial caudal direction from the puncture site. In all the animals, there was sufficient staining of the brachial plexus root at site P1. There was also complete staining of the cranial pectoral, suprascapular, subscapular, musculocutaneous, axillary, median, ulnar, and radial nerves at site P2, which produced a high staining score with US (2/12= 25% partially= 75% completely stained and segment of stained nerve = 2cm).

Experimental live study

The greater tuberosity of humerus appeared as hyperechoic structure from the ultra-sonographic appearance, with the deep and superficial pectoral muscles appearing as hypoechoic. The axillary artery and vein were colored as hypoechoic region, and the ultra-sonographic test showed the pulsation of the artery (Fig. 5). From the ultra-sonographic image before injection, the brachial

plexus appeared as a hyperechoic cluster at site P1. After injection, it became hypoechoic with a hyperechoic rounded area at site P2. In all cases, to reach the brachial plexus at site p1, the needle travelled 4.8±0.2cm delivering 10ml of lidocaine of local anesthetic solution to the blockage. To reach site P2 the needle covered about 6.8±0.2 cm delivering 20 ml of the local anesthetic to achieve complete blockage of the nerve (Fig. 6). The signs of arthritis were identified by the extent of muscular relaxation, the inability of the carpal and elbow joints to bear weight, loss of sensation at the forelimb, as well as complete irresponsiveness during any surgical approaches of the forelimb (Fig. 7).
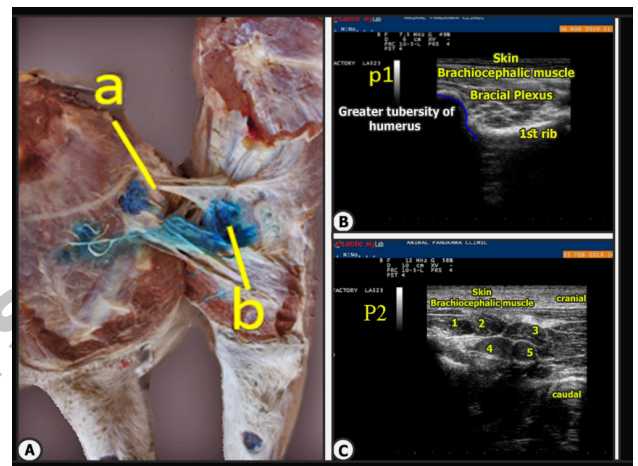

Fig. 4. Gross anatomical (A) and ultrasound view to determine the US-guided cadaver study at sites p1 (B) and p2 (C).
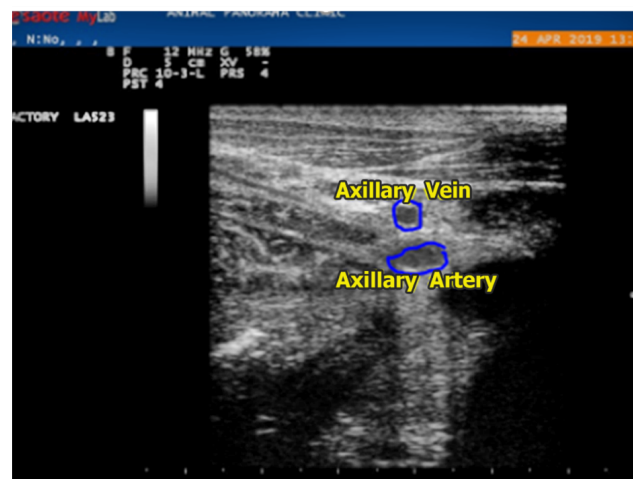

Fig. 5. Ultrasonogram of the brachial plexus region in longitudinal transducer in life beneath the muscle demonstrating the brachial blood vessels.
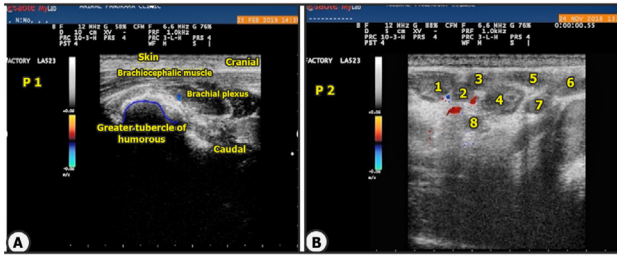
Fig. 6. Ultrasonogram of the brachial plexus region in longitudinal transducer in life beneath the muscle demonstrating the injected brachial plexus at site p1 (A) and site p2 (B).
Abbreviation: 1, musculocutaneous nerve; 2, median nerve; 3, the ulnar nerve; 4, redial nerve; 5, axillary nerve; 6, lateral thoracic nerve; 7, suprascapular nerve and 8, subscapular nerve.

Fig. 7. The donkey showed scapula-humeral angle and was unable to bear weight after the injected forelimb with lidocaine 2%.

DISCUSSION

Anatomical study

The shoulder area was dissected specifically at the cranial border, to identify the muscular, blood vessel, and brachial plexus architecture. The brachial plexus is located inferior to the brachiocephalic muscle; with its cranial part identified as the plexus root, while the caudal part is the plexus nerves. The largest ventral nerves consists of the axillary, musculocutaneous, radial, ulnar, and median nerves that supply the forelimb, while the long lateral thoracic, cranial-caudal pectoral, supra- and sub-scapular, and thoracodorsal nerves make up the caudal-dorsal nerves that supply the rest of the shoulder region (Campoy *et al.*, 2010).

The best position to reach the brachial plexus is above the greater tuberosity, and this area is split into two partitions (P1 and P2) that meet at P1 and P2, 2±0.5 cm and 4±0.5 cm above the humeral tuberosity, respectively (Iwamoto *et al.*, 2012). During the dissection, the axillary artery is located before the plexus at the cranial border at site P1. This is often considered one of the disadvantages of P1 because of the possibility of complications (Skarda, 1996; Valverde and Sinclair, 2015). In this study, the needle travelled about 5±0.5 cm to reach site P1 of the brachial plexus, passing through the skin, pectoral muscle, sternocephalic and brachiocephalic muscles, fat, and connective tissue. To reach site P2, the needle travelled 7±1.0 cm through the structures. The distance for P2 was greater than P1 because of the caudal divisions of the plexus (Iwamoto *et al.*, 2012).

Cadaveric study

In this study, the doppler ultrasound with an 8 MHz linear transducer produced images at site P1 that appeared as a cluster of hyperechoic structures, indicating the root of the brachial plexus. The axillary blood vessels appeared as a hyperechoic rim, cranial to the root of the plexus, whereas at site P2 there were multiple hyperechoic areas encircled by a hyperechoic structure having multiple discontinuous lines. The results were comparable to the peripheral nerve US images illustrated in humans and small animals (Echeverry *et al.*, 2010; Guilherme and Benigni, 2008; Iwamoto *et al.*, 2012; Rodrigo-Mocholi and Martinez-Taboada, 2020). The root of the brachial plexus was seen with large branches of the axillary artery and vein when the probe was placed longitudinally in P1. At P2, the peripheral nerves were seen after dorsally moving the probe several centimeters. Therefore, it was feasible to see the needle and tip moving to the area just outside of the brachial plexus and conducting the brachial plexus block while being guided by the US. With the needle moving craniocaudally, the origin of the plexus is more superficial to the skin, and the needle advancement to P1 was 4.8±0.4 cm, while at P2, the probe travelled 6.8±0.2 cm to reach the plexus division.

The use of direct visualization of the brachial plexus, the peripheral nerves, and its surrounding structure during the injection of methylene blue produced results with high precision and success rate in both sites; P1 and P2 (Iwamoto *et al.*, 2012). The directly injected dye to the plexus resulted in complete (100%) staining of all brachial plexus nerves at site P1 because the stain reaching the root

of the plexus (Adams, 2004; Campoy *et al*., 2010), while at P2 the staining was 75% complete because of the poor staining of the dorsal and ventral division of the plexus. The use of color Doppler US-guided technique provides clear discrimination of the brachial plexus from the branches of the axillary artery and vein under, and reduces the risk of damaging the vessels by direct puncture (Iwamoto *et al*., 2012).

Live experimental study

The caudal nerves are the most significant rami to be included in the brachial plexus block to desensitize the distal thoracic limb (Skelding *et al*., 2018). This is due to the fact that they are the primary sources of the radial, ulnar, and median nerves (Campoy *et al*., 2010). The dose of local anesthetics injected in the current study was 15 ml of lidocaine at 2% per donkey at site P1 while it was 25 ml of lidocaine at 2% at site P2, since ultrasonography allows the target nerve and encircling structures to be visualized, the needle tip position to be evaluated, and local anesthetic spread to be visualized (Souto *et al*., 2020). In contrast, 25-40 ml of 2% lidocaine is used in a conventional brachial plexus block in equine medicine (Neal, 2010; Skarda, 1996).

In clinical studies, because of the injection of local anesthetic agent into the root of the plexus, a propensity for a faster onset and longer duration of block action was observed for nerves in site P1 of the brachial plexus compared to nerves in site P2 (Iwamoto *et al*., 2012). Clinically, after 15±2 mins at site P1, the donkey cannot bear weight on the fore limb versus 20±2 mins at P2. Compared to the onset of analgesia with the conventional approach, this time of onset was considered short, averaging 15-30 mins due to the direct spread of analgesics around the plexus. After lidocaine injection, the high success rate of lidocaine was observed, leading to complete brachial block. Due to the direct introduction of local anesthetics around the nerve, the block was confirmed by the irresponsiveness to the pinprick test and the incision made at the metacarpal area at both sites. The imaging did not reveal any complication following the brachial plexus blockade in the live animal, as the axillary blood vessels appeared colored and pulsatile (Campoy *et al*., 2010). The use of the doppler US assist in monitoring the process; however, to achieve successful blockade of the nerves, the critical length of nerve should receive sufficient concentration of the local anesthetic solution (Campoy *et al*., 2010).

The pain score is the 120 min sum of the scores, and the analgesic effect is recorded when the pain score is 2 (complete analgesia effect). That analgesic effect started at sites P1 and P2 after 15 min and continued for 100±15 mins at P1 and P2 for 90±15 min at P2 from which animals recovered from low pain score anesthesia of 0. Due to the direct introduction of the analgesia around the nerve root of the plexus, the total distribution time of analgesia at P1 was 120 mins compared to 105 mins at P2 (Iwamoto *et al*., 2012). These techniques did not only reduce the disadvantages of general anesthesia, but they led to efficient anaesthetization.

CONCLUSION

Using color Doppler US-guided brachial plexus injection, site P1 was more efficient and avoided vascular penetration than site P2. The caudal approach appears to be most appropriate for providing a sufficient nerve block with minimized risk of complications because the injected agent spreads efficiently around the target nerves with a rapid onset of anesthesia at lower dose. The risk of injury to the brachial vessels is reduced, since the needle is visualized and be monitored in real-time.

ACKNOWLEDGMENT

Data availability statement
Research data are not shared

Statement of conflict of interest
The authors have declared no conflict of interest.

REFERENCES

Adami, C., and Studer, N., 2015. A case of severe ventricular arrhythmias occurring as a complication of nerve-stimulator guided brachial plexus location. *Vet. Anaesth. Analg*., **42**: 230-231. https://doi.org/10.1111/vaa.12236

Adams, D.R., 2004. *Canine anatomy: A systemic study*. Iowa State Press.

Atiba, A.S., Ghazy, A., Farrag, F.A., El-Magd, M.A. and Almadaly, E.A., 2019. Ultrasound-guided brachial plexus nerve block in donkeys. *Slovenian Vet. Res*., **56**(**Suppl. 22**): 7-14. https://doi.org/10.26873/SVR-739-2019

Bennett, R.J., Wooten, A., Babbel, L. and Reel, B.A., 2020. Horner's syndrome with unilateral brachial plexus blockade mimicking cerebrovascular accident following lumbar combined spinal epidural analgesia for labor. *Mil. Med*., **185**: e322-e323. https://doi.org/10.1093/milmed/usz160

Bhalla, R.J., and Leece, E.A., 2015. Pneumothorax following nerve stimulator-guided axillary brachial plexus block in a dog. *Vet. Anaesth. Analg.*, **42**: 658-659. https://doi.org/10.1111/vaa.12288

Brull, R., Perlas, A. and Chan, V.W.S., 2007. Ultrasound-guided peripheral nerve blockade. *Curr. Pain Headache Rep.*, **11**: 25-32. https://doi.org/10.1007/s11916-007-0018-6

Campoy, L., Bezuidenhout, A.J., Gleed, R.D., Martin-Flores, M., Raw, R.M., Santare, C.L., Jay, A.R. and Wang, A.L., 2010. Ultrasound-guided approach for axillary brachial plexus, femoral nerve, and sciatic nerve blocks in dogs. *Vet. Anaesth. Analg.*, **37**: 144-153. https://doi.org/10.1111/j.1467-2995.2009.00518.x

Dyce, K.M., Sack, W.O., and Wensing, C.J.G., 2010. *Textbook of veterinary anatomy.* 5th edition, W.B. Saunders Company, Philadelphia, London and Toronto.

Echeverry D.F., Gil F., Laredo F., Ayala, M.D., Belda, E., Soler, M. and Agut, A., 2010. Ultrasound-guided block of the sciatic and femoral nerves in dogs: A descriptive study. *Vet. J.,* **186**: 210-215. https://doi.org/10.1016/j.tvjl.2009.08.005

Food and Agriculture Organization of the United Nations F, 2021. Crops and livestock products trade data. *FAOSTAT Stat. Datab.*, http://www.fao.org/faostat/en/#data/QCL/visualize. Retrieved from

Guilherme, S., and Benigni, L., 2008. Ultrasonographic anatomy of the brachial plexus and major nerves of the canine thoracic limb. *Vet. Radiol. Ultrasound,* **49**: 577-583. https://doi.org/10.1111/j.1740-8261.2008.00424.x

Holzman, R.S., 2002. Unilateral horner's syndrome and brachial plexus anesthesia during lumbar epidural blockade. *J. clin. Anesth.*, **14**: 464-466. https://doi.org/10.1016/S0952-8180(02)00399-9

Iwamoto, J., Yamagishi, N., Sasaki, K., Kim, D., Devkota, B. and Furuhama, K., 2012. A novel technique of ultrasound-guided brachial plexus block in calves. *Res. Vet. Sci.*, **93**: 1467-1471. https://doi.org/10.1016/j.rvsc.2012.05.010

Lemke, K.A., and Creighton, C.M., 2008. Paravertebral blockade of the brachial plexus in dogs. *Vet. Clin. North Am. Small Anim. Pract.*, **38**: 1231-1241. https://doi.org/10.1016/j.cvsm.2008.06.003

Mahler, S.P., and Adogwa, A.O., 2008. Anatomical and experimental studies of brachial plexus, sciatic, and femoral nerve-location using peripheral nerve stimulation in the dog. *Vet. Anaesth. Analg.*, **35**: 80-89. https://doi.org/10.1111/j.1467-2995.2007.00356.x

Marhofer, P., Greher, M. and Kapral, S., 2005. Ultrasound guidance in regional anaesthesia. *Br. J. Anaesth.*, **94**: 7-17. https://doi.org/10.1093/bja/aei002

Marhofer, P., Schrogendorfer, K., Koinig, H., Kapral, S., Weinstabl, C. and Mayer, N., 1997. Ultrasonographic guidance improves sensory block and onset time of three-in-one blocks. *Anesth. Analg.*, **85**: 854-857. https://doi.org/10.1097/00000539-199710000-00026

Mirza, F., and Brown, A.R., 2011. Ultrasound-guided regional anesthesia for procedures of the upper extremity. *Anesthesiol. Res. Pract.*, **2011**. https://doi.org/10.1155/2011/579824

Monticelli, P., Fitzgerald, E., and Viscasillas, J., 2018. A sonographic investigation for the development of ultrasound-guided paravertebral brachial plexus block in dogs: Cadaveric study. *Vet. Anaesth. Analg.*, **45**: 195-202. https://doi.org/10.1016/j.vaa.2017.08.005

Neal, J.M., 2010. Ultrasound-guided regional anesthesia and patient safety: An evidence-based analysis. *Reg. Anesth. Pain med.*, **35**(**Suppl 1**): S59-S67. https://doi.org/10.1097/AAP.0b013e3181ccbc96

Norris, S.L., Little, H.A., Ryding, J. and Raw, Z., 2021. Global donkey and mule populations: Figures and trends. *PLoS One*, **16**: e0247830. https://doi.org/10.1371/journal.pone.0247830

Raw, R.M., Read, M.R., and Campoy, L., 2013. Peripheral nerve stimulators. In: *Small Animal Regional Anaesthesia and Analgesia* (eds. L. Campoy and M.R. Read). Wiley Blackwell, Ames, IA, USA. pp. 65–76.

Rodrigo-Mocholi, D., and Martinez-Taboada, F., 2020. Novel ultrasound-guided lateral approach for femoral nerve block in cats: A pilot study. *J. Feline Med. Surg.,* **22**: 339-343. https://doi.org/10.1177/1098612X19845719

Skarda, R.T., 1996. Local and regional anesthesia in ruminants and swine. *Vet. Clin. N. Am. Fd. Anim. Pract.*, **12**: 579-626. https://doi.org/10.1016/S0749-0720(15)30390-X

Skelding, A., Valverde, A., Sinclair, M., Thomason, J. and Moens, N., 2018. Anatomical characterization of the brachial plexus in dog cadavers and comparison of three blind techniques for blockade. *Vet. Anaesth. Analg.*, **45**: 203-211. https://doi.org/10.1016/j.vaa.2017.11.002

Souto, M.T.M., Fantoni, D.T., Hamaji, A., Hamaji, M., Vendruscolo, C.P., Otsuki, D.A., Pinto, A.C.B. and Ambrósio, A.M., 2020. Ultrasound-guided continuous block of median and ulnar nerves in

A. Sobhy *et al.*

horses: Development of the technique. *Vet. Anaesth. Analg.*, **47**: 405-413. https://doi.org/10.1016/j.vaa.2019.12.008

Tsui, B.C., Doyle, K., Chu, K., Pillay, J. and Dillane, D., 2009. Case series: Ultrasound-guided supraclavicular block using a curvilinear probe in 104 day-case hand surgery patients. *Can. J. Anesth.* *J. Can. Anesth.,* **56**: 46-51. https://doi.org/10.1007/s12630-008-9006-5

Valverde, A., and Sinclair, M., 2015. 51 ruminant and swine local anesthetic and analgesic techniques. *Vet. Anesth. Analg.*, **941**: 51. https://doi.org/10.1002/9781119421375.ch51